Contemporary Mathematics
https://ojs.wiserpub.com/index.php/CM/

Research Article

Modeling the Cyclic Dynamics of a Tyrosinase-Based Catechol Sensor

Dorathy Cathrine A.[1], Raja R.[2], Swaminathan R.[1]*

[1] PG & Research Department of Mathematics, Vidhyaa Giri College of Arts and Science (Affiliated to Alagappa University), Puduvayal, Tamil Nadu, 630 108, India
[2] Ramanujan Centre for Higher Mathematics, Alagappa University, Karaikudi, Tamil Nadu, 630 003, India
E-mail: swaminathanmath@gmail.com

Received: 11 September 2025; **Revised:** 20 October 2025; **Accepted:** 31 October 2025

Abstract: A cyclic redox reaction, mediated by L-ascorbic acid and involving catechol and 1,2-benzoquinone, forms the basis of the mathematical model developed for a tyrosinase-based amperometric biosensor. The system is governed by a ping-pong bi-bi mechanism and modeled using nonlinear reaction-diffusion equations under steady-state conditions. The Homotopy Perturbation Method (HPM) is applied to derive approximate analytical solutions, which show excellent agreement with numerical results. The effects of key dimensionless parameters, particularly the Thiele modulus, are analysed to assess sensor performance. Results highlight the critical balance between reaction kinetics and diffusion in determining sensitivity and current response. The proposed model provides a valuable analytical tool for optimising biosensor design in both clinical and environmental applications.

Keywords: mathematical modeling, cyclic reaction, catechol sensor, nonlinear differential equation, boundary value problems

MSC: 34A34, 34B15, 34B18, 34B60

Nomencleature

Symbols		Units
$[S]$	Measured substrate concentration of catechol	mM
$[L]$	Medial product concentration of 1,2-benzoquinone	mM
$[R]$	Reducing agent concentration of L-ascorbic acid	mM
$[C]$	Co-substrate concentration of oxygen	mM
V_m	Maximal rate	mmol/L_s
D_S	Diffusion coeffiscient for substrate	m^2/s
D_L	Diffusion coefficient for medial product	m^2/s
D_R	Diffusion coefficient for reducing agent	m^2/s
D_C	Diffusion coefficient for co-substrate	m^2/s
$K_2,\ K_3,\ K_4,\ K_m$	Reaction rate constant	mmol/L_s

DOI: https://doi.org/10.37256/cm.7220268595

K_s, K_C	Reaction rate constant	mM
δ	Distance coordinate	μm
d	Active member thickness	
h	Convergence control parameter	dimensionless
S	Normalised measured substrate concentration	dimensionless
L	Normalised medial product concentration	dimensionless
R	Normalised reducing agent concentration	dimensionless
C	Normalised co-substrate concentration	dimensionless
x	Normalised distance coordinator	
α, β, γ, λ	Saturation parameters	dimensionless
m_1, m_2, m_3	Linear enzyme kinetic coefficient	dimensionless
μ_1, μ_2, μ_3	Ratio of diffusion coefficients	dimensionless
ρ, ρ_1	Ratio of reaction rate constants	dimensionless
φ^2	Thiele modulus	dimensionless
Ψ	Normalised current	dimensionless

1. Introduction

Amperometric biosensors represent a cornerstone of modern analytical chemistry, finding extensive application in biomedical diagnostics, environmental monitoring, and biotechnology owing to their high sensitivity, selectivity, and rapid response times [1–3]. The operational principle of these devices hinges on the measurement of current generated from the redox reactions of target analytes, typically facilitated by immobilised enzymes.

A prominent strategy for enhancing the performance of these sensors involves the implementation of cyclic reaction schemes [4, 5]. In such systems, the enzymatic conversion of a substrate to an electroactive product is coupled with its subsequent regeneration, often via a second enzyme or a chemical mediator. This catalytic cycle enables multiple turnovers of the analyte per recognition event, leading to significant signal amplification and lower detection limits [6]. Accurately modeling these systems is complex, requiring a detailed description of reaction kinetics, mass transport, and electrochemical boundary conditions.

Mathematical modeling is indispensable for optimizing biosensor design, as it elucidates the critical interplay between enzymatic activity and diffusion. While numerical methods are frequently employed to solve the underlying nonlinear differential equations [7], analytical solutions offer distinct advantages, including enhanced physical insight, computational efficiency, and avoidance of numerical artefacts [8]. Nevertheless, deriving such solutions for intricate cyclic reactions remains a challenge due to the inherent nonlinearity of the governing equations.

We develop an analytical model for a tyrosinase biosensor utilizing an L-ascorbic acid-mediated catechol/1,2-benzoquinone redox cycle. The system is governed by a ping-pong bi-bi mechanism and modeled using nonlinear reaction-diffusion equations under steady-state conditions. We apply the Homotopy Perturbation Method (HPM) [9] to derive approximate analytical solutions for the concentration profiles of all reacting species and the resulting current. The analytical results are validated against numerical simulations, demonstrating excellent agreement. A parametric study is conducted to assess the influence of key dimensionless parameters, particularly the Thiele modulus, on sensor behaviour. The proposed model provides a valuable theoretical framework for the rational design and optimisation of enzymatic biosensors in clinical and environmental applications.

2. Problem modeling and analytical derivation

2.1 *Mathematical formulation and reaction scheme*

The biosensor employs a pre-treated potato tissue membrane, free of endogenous phenols, immersed in a catechol (S_0) and L-ascorbic acid (R_0) solution. Oxygen (C_0) from ambient air serves as the co-substrate. Within the membrane,

a cyclic reaction occurs (Figure 1): tyrosinase catalyzes the oxidation of catechol (S) to 1,2-benzoquinone (L), which is then chemically reduced back to catechol by L-ascorbic acid (R), forming dehydroascorbic acid (P_2). This catalytic cycle amplifies the sensor's current response but results in a net depletion of dissolved oxygen, as oxygen is not regenerated during reduction.

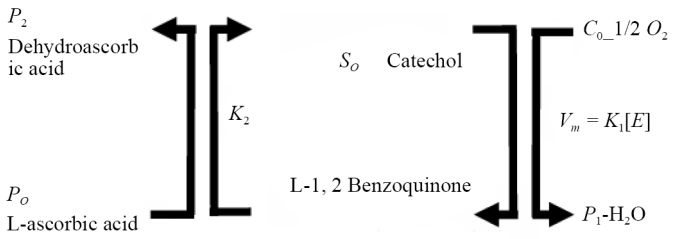

Figure 1. A schematic illustration of the core cyclic reaction mechanism underlying the biosensor's operation

The kinetics follow a ping-pong bi-bi mechanism, represented as [10]:

$$S + C \xrightarrow{K_1} L + P_1; \text{ (A)}$$

$$l + R \xrightarrow{K_2} S + P_2. \text{ (B)}$$

Here, K_1 and K_2 are the rate constants for the enzymatic and chemical steps, respectively. Catechol (S) acts as the substrate, oxygen (C) as the co-substrate, and L-ascorbic acid (R) as the reducing agent. This two-step enzymatic-chemical process (A) and (B) forms a self-sustaining cycle that continues until the available oxygen is consumed.

Under steady-state conditions, the ping-pong mechanism is governed by the following system of differential equations [11]

$$D_S \frac{d^2[S]}{d\delta^2} = \frac{V_m}{1 + \left(\frac{K_S}{[S]} + \frac{K_C}{[C]}\right)} - \frac{K_2[L][R]}{{K_m}^2} \tag{1}$$

$$D_L \frac{d^2[L]}{d\delta^2} = \frac{V_m}{1 + \left(\frac{K_S}{[S]} + \frac{K_C}{[C]}\right)} \frac{K_3[L]}{K_m} \tag{2}$$

$$D_R \frac{d^2[R]}{d\delta^2} = \frac{K_4[R]}{K_m} \tag{3}$$

$$D_C \frac{d^2[C]}{d\delta^2} = \frac{V_m}{1 + \left(\frac{K_S}{[S]} + \frac{K_C}{[C]}\right)}. \tag{4}$$

The system's boundary conditions are

$$[S] = S_0,\ [L] = L_0,\ [R] = R_0,\ [C] = C_0 \quad \text{when } \delta = 0; \tag{5}$$

$$\frac{d[S]}{d\delta} = 0,\ \frac{d[L]}{d\delta} = 0,\ \frac{d[R]}{d\delta} = 0,\ [C] = 0 \quad \text{when } \delta = d. \tag{6}$$

The diffusion-limited current is given by the following expression where n is the number of electrons transferred in the electrochemical reaction at the cathode, F is the Faraday constant, A is the electrode area, and D_C is the diffusion coefficient of catechol:

$$I = nFAD_C \left(\frac{d[C]}{d\delta} \right)_{\delta=d}. \tag{7}$$

The transition to a non-dimensional formulation serves to reduce the number of free parameters and reveal the fundamental scaling relationships that govern the system's dynamics. The model is non-dimensionalised using characteristic scales inherent to the biosensor's operation.

2.2 *Non dimensional formulation*

By defining these non-dimensional parameters

$$x = \frac{\delta}{d} : S = \frac{[S]}{K_S} :: L = \frac{[L]}{K_m} :: R = \frac{[R]}{K_m};\ C = \frac{C}{K_C}$$

$$\varphi^2 = \frac{d^2 V_m}{D_S K_m};\ \rho = \frac{K_m}{K_C};\ \rho_1 = \frac{K_m}{K_S} : \alpha = \frac{S_0}{K_S}$$

$$\beta = \frac{C_0}{K_C};\ \gamma = \frac{R_0}{K_m};\ \lambda = \frac{L_0}{K_m};$$

$$m_1 = \frac{K_2}{V_m};\ m_2 = \frac{K_3}{V_m};\ m_3 = \frac{K_4}{V_m}$$

$$\mu_1 = \frac{D_S}{D_C};\ \mu_2 = \frac{D_S}{D_L};\ \mu_3 = \frac{D_S}{D_R}. \tag{8}$$

The dimensional governing equations (1)-(4) and their associated boundary conditions (5) and (6) are now cast in dimensionless form using the parameters defined above

$$\frac{d^2 s}{dx^2} = \varphi^2 \rho_1 \left[\left(1 + \frac{1}{s} + \frac{1}{c} \right)^{-1} - m_1 LR \right] \tag{9}$$

$$\frac{d^2L}{dx^2} = \varphi^2\mu_2\left[m_2L - \left(1+\frac{1}{S}+\frac{1}{C}\right)^{-1}\right] \tag{10}$$

$$\frac{d^2R}{dx^2} = \mu_3 m_3 \varphi^2 R \tag{11}$$

$$\frac{d^2C}{dx^2} = \varphi^2\mu_1\rho\left[\left(1+\frac{1}{s}+\frac{1}{C}\right)^{-1}\right]. \tag{12}$$

This leads to the following transformed boundary conditions

$$S = \alpha,\ L = \lambda,\ R = \gamma,\ C = \beta \quad \text{when } x = 0 \tag{13}$$

$$\frac{ds}{dx} = 0,\ \frac{dL}{dx} = 0,\ \frac{dR}{dx} = 0,\ C = 0 \quad \text{when } x = 1. \tag{14}$$

The dimensionless current is

$$\Psi = \frac{Id}{nFAD_cK_c} = \left(\frac{dc}{dx}\right)_{x=1}. \tag{15}$$

3. Approximate analytical solutions for the concentration dynamics of four reactants: a homotopy perturbation approach

Generally, obtaining exact solutions for nonlinear differential equations that arise in modeling real-world physical phenomena remains a challenging task. However, significant progress has been made in recent decades through the development of highly accurate approximate analytical methods. Among the most prominent techniques are the Taylor series method [12], the Variational Iteration Method (VIM) [13], and Greens function Iterative approach [14]. Other effective methodologies include the residual method [15], the hyperbolic function method, Padé approximation [16], Homotopy Analysis method [17], the Adomian decomposition method [18], and Akbari-Ganji's method [19, 20]. These analytical approaches have proven particularly valuable for solving complex nonlinear problems where exact solutions are often intractable.

The HPM, introduced by He in 1999 [21, 22] has emerged as one of the most widely adopted techniques for solving nonlinear systems across various scientific and engineering disciplines. Applying this method to equations (9)-(14) yields the following approximate analytical solutions for the dimensionless concentration profiles of the reactants (detailed derivations are provided in Appendix A):

$$S(x) = \alpha + \varphi^2\rho_1\left(\frac{-\alpha\beta}{\alpha\beta+\alpha+\beta} + m_1\lambda\gamma\right)\left(x - \frac{x^2}{2}\right) \tag{16}$$

$$L(x) = \lambda + \varphi^2 m_2\left(\frac{\alpha\beta m_2 + \alpha\lambda m_2 + \beta\lambda m_2 - \alpha\beta}{\alpha\beta+\alpha+\beta}\right)\left(\frac{x^2}{2} - x\right) \tag{17}$$

$$R(x) = \gamma + \varphi^2 m_3 \mu_3 \gamma \left(x^2 - x\right) \tag{18}$$

$$C(x) = -\beta x + \beta + \left(\frac{\varphi^2 \mu_1 \rho \alpha \beta}{(\beta+1)\alpha + \beta}\right)\left(\frac{x^2}{2} - x\right). \tag{19}$$

Using (15) and (19) we obtain the current as follows

$$\text{Current } \Psi = \left(\frac{dc}{dx}\right)_{x=1} = -\beta. \tag{20}$$

4. Result and discussion

To assess the accuracy of the proposed analytical approach with a finite number of terms, the system of differential equations (9)-(12) was also solved using numerical techniques. The nonlinear differential equations were solved numerically using the built-in pdepe function in Scilab/Matlab, which implements the finite element method. The results of the proposed analytical method are validated against these numerical solutions in Tables 1-4 and Figures 2-6, demonstrating strong agreement. The average relative errors between the analytical and numerical results are found to be 0.17%, 0.09%, 0.12% and 0.48% for the concentrations of substrate, co-substrate, reducing agent, and intermediate product, respectively.

Table 1. Normalized substrate concentration $S(x)$ versus spatial coordinate x for varying Thiele modulus φ^2. Fixed parameters: $\alpha = 0.09$, $m_1 = 2$, $\rho_1 = 0.5$

X	$\varphi^2 = 0.01$			$\varphi^2 = 0.5$			$\varphi^2 = 1$		
	Numerical Value (NUM)	HPM	Error Percentage (ERR)	NUM	HPM	ERR	NUM	HPM	ERR
0	0.09	0.09	0	0.09	0.09	0	0.09	0.09	0
0.2	0.091	0.0909	0.11	0.1192	0.1182	0.84	0.1499	0.15	0.07
0.4	0.0917	0.0915	0.22	0.1418	0.142	0.14	0.1944	0.1942	0.10
0.6	0.0923	0.092	0.33	0.1579	0.158	0.06	0.2255	0.2254	0.04
0.8	0.0926	0.0923	0.32	0.1674	0.1675	0.06	0.2446	0.2445	0.04
1	0.0927	0.0924	0.32	0.1704	0.1705	0.06	0.2518	0.2517	0.04
	Average (AVG) ERR %		0.27	AVG ERR %		0.19	AVG ERR %		0.05

Table 2. Normalized Reducing agent concentration $L(x)$ versus spatial coordinate x for varying Thiele modulus φ^2. Fixed parameters: $\lambda = 0.09$, $m_2 = 2$, $\mu_2 = 0.5$

X	$\varphi^2 = 0.1$			$\varphi^2 = 0.3$			$\varphi^2 = 0.5$		
	NUM	HPM	ERR	NUM	HPM	ERR	NUM	HPM	ERR
0	0.5	0.5	0	0.5	0.5	0	0.5	0.5	0
0.2	0.4968	0.4965	0.06	0.4903	0.4903	0	0.4838	0.4842	0.08
0.4	0.4942	0.4938	0.08	0.4827	0.4827	0	0.4712	0.4718	0.13
0.6	0.4925	0.4912	0.26	0.4774	0.4768	0.13	0.4623	0.4628	0.11
0.8	0.4914	0.4905	0.18	0.4742	0.4733	0.19	0.457	0.4572	0.04
1	0.4911	0.4901	0.20	0.4732	0.4721	0.23	0.4554	0.4555	0.02
	AVG ERR %		0.13	AVG ERR %		0.09	AVG ERR %		0.06

Table 3. Normalized Reducing agent concentration $R(x)$ versus spatial coordinate x for varying Thiele modulus φ^2. Fixed parameters: $\gamma = 1$, $m_3 = 0.1$, $\mu_3 = 0.6$

X	$\varphi^2 = 0.5$			$\varphi^2 = 1$			$\varphi^2 = 5$		
	NUM	HPM	ERR	NUM	HPM	ERR	NUM	HPM	ERR
00	1	1	0	1	1	0	1	1	0
0.2	0.9946	0.9946	0	0.9893	0.9891	0.02	0.9515	0.9455	0.63
0.4	0.9903	0.9903	0	0.981	0.9807	0.03	0.9146	0.9133	0.14
0.6	0.9873	0.9873	0	0.9752	0.9747	0.05	0.8888	0.8833	0.62
0.8	0.9855	0.9856	0.01	0.9717	0.9711	0.06	0.8739	0.8725	0.16
1	0.9849	0.985	0.01	0.9706	0.97	0.06	0.8695	0.868	0.17
	AVG ERR %		0.02	AVG ERR %		0.04	AVG ERR %		0.29

Table 4. Normalized co-substrate concentration $C(x)$ versus spatial coordinate x for varying Thiele modulus φ^2. Fixed parameters: $\beta = 0.5$, $\rho = 0.1$, $\mu_1 = 0.8$

X	$\varphi^2 = 0.1$			$\varphi^2 = 1$			$\varphi^2 = 5$		
	NUM	HPM	ERR	NUM	HPM	ERR	NUM	HPM	ERR
0	0.54	0.54	0	0.54	0.54	0	0.54	0.54	0
0.2	0.431	0.4304	0.14	0.3897	0.3902	0.13	0.3573	0.3555	0.50
0.4	0.3224	0.3215	0.28	0.2623	0.2624	0.04	0.22	0.2209	0.41
0.6	0.214	0.2119	0.98	0.1582	0.1587	0.32	0.1237	0.1227	0.81
0.8	0.1059	0.1049	0.94	0.0735	0.074	0.68	0.0574	0.0577	0.52
1	0.003	0.003	0	0.004	0.004	0	0.01	0.01	0
	AVG ERR %		0.39	AVG ERR %		0.68	AVG ERR %		0.37

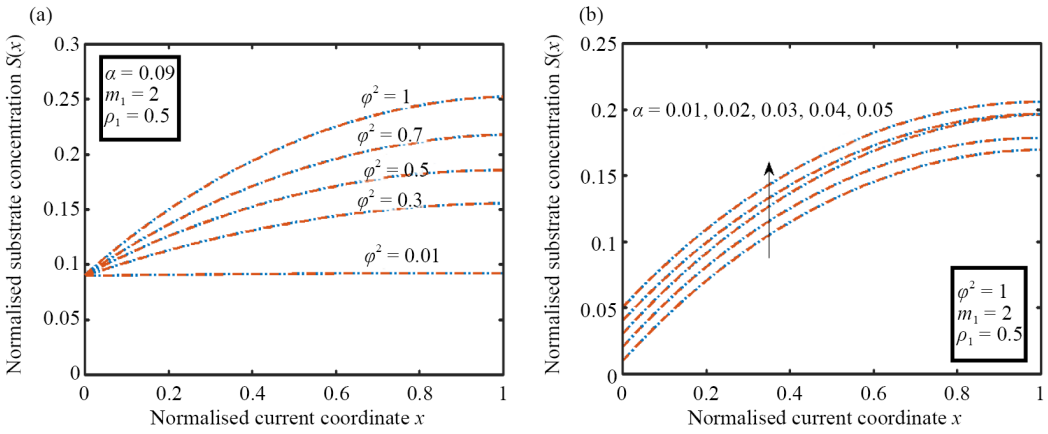

Figure 2. Variation of normalized substrate concentration $S(x)$ along the normalized current coordinate x

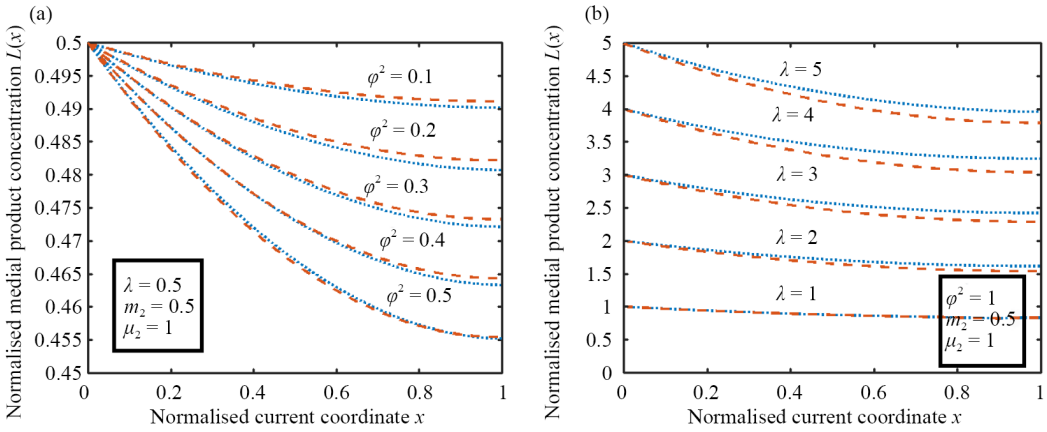

Figure 3. Profiles of normalised medial product concentration $L(x)$ versus normalised spatial coordinate x

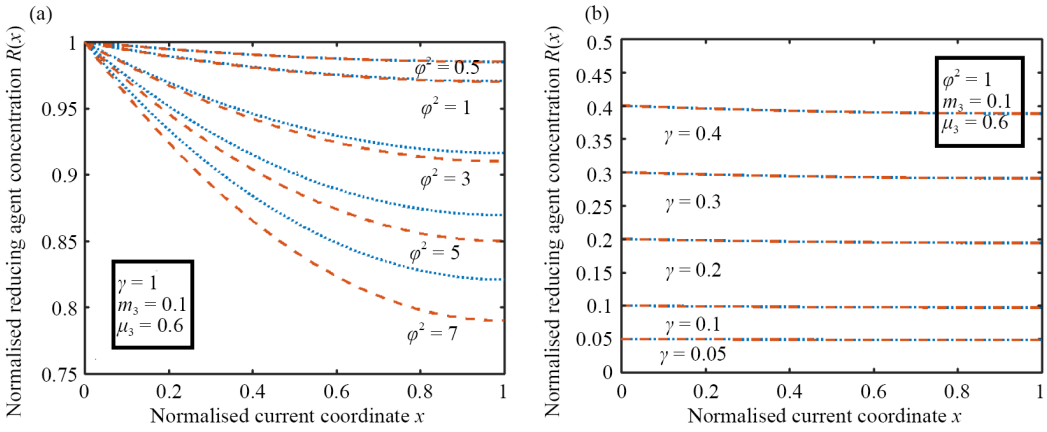

Figure 4. Illustrate the normalized concentration profiles of a reducing agent, $R(x)$ as a function of the normalized current coordinate x, under varying dimensionless parameters

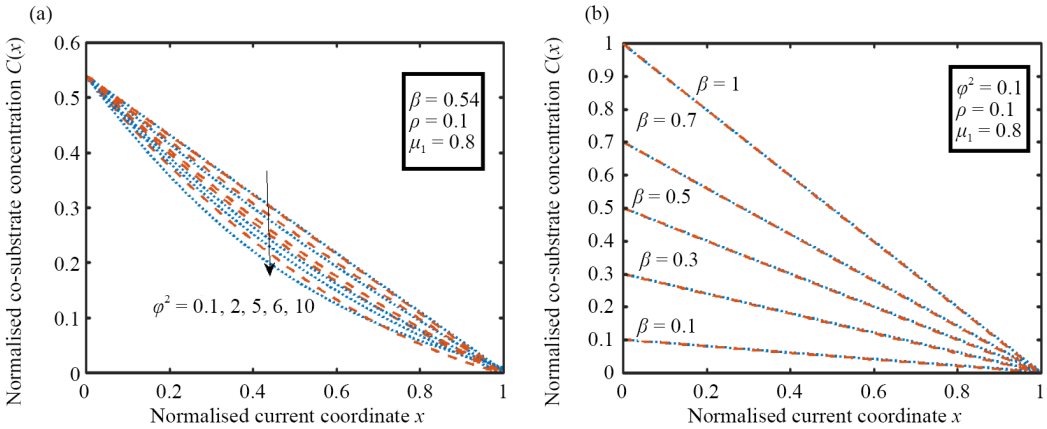

Figure 5. Depict the variation of the normalised co-substrate concentration $C(x)$ along the normalised current coordinate x for different parameter settings

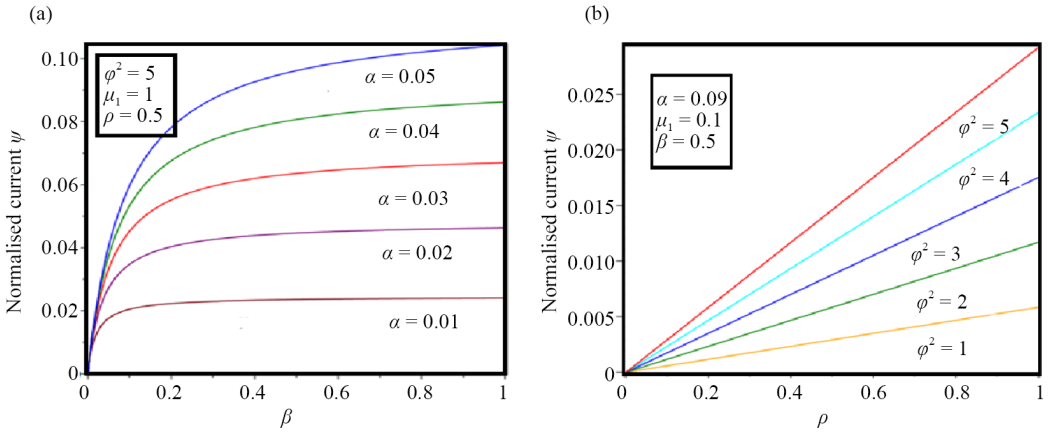

Figure 6. Illustrate the behaviour of the normalised current Ψ as influenced by different dimensionless parameters in a porous catalytic system

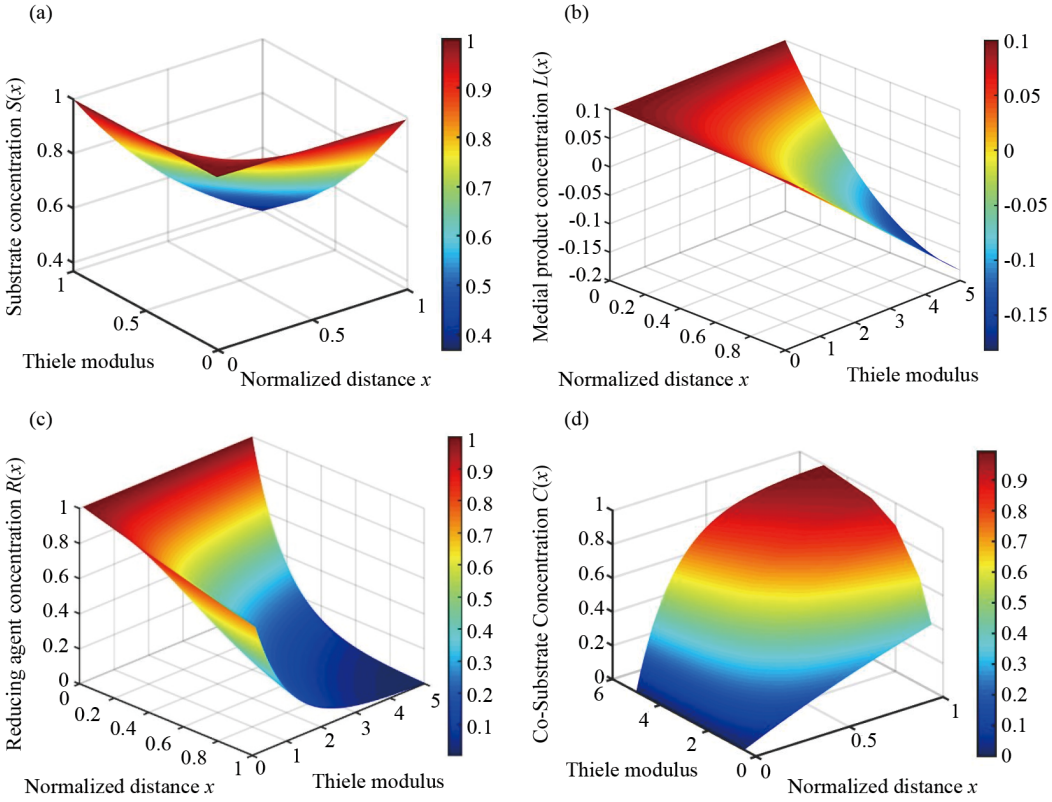

Figure 7. Three-dimensional representations of the concentration profiles of substrate, mediator, product, and co-substrate as functions of Thiele modulus φ and dimensionless distance (x), highlighting the influence of diffusion and reaction kinetics within the bio-catalytic system

Figure 7a presents the three-dimensional profile of substrate concentration $S(x)$, demonstrating a symmetric decline across the domain. The depletion becomes more pronounced with increasing Thiele modulus φ, which represents the ratio of the intrinsic reaction rate to the diffusion rate. A higher φ indicates stronger internal diffusion resistance, thereby limiting substrate penetration and utilization within the reactive medium. Figure 7b shows the distribution of medial product concentration $L(x)$, which progressively decreases with spatial depth and increasing φ. The emergence of negative concentrations suggests transformation or consumption of intermediate species under diffusion-limited conditions. In

Figure 7c, the reducing agent concentration $R(x)$ exhibits a steady decline along the spatial coordinate, with sharper reductions at higher φ, reflecting enhanced consumption and reduced replenishment. Figure 7d illustrates the co-substrate concentration $C(x)$, which generally increases with spatial progression but diminishes as φ increases, highlighting the critical role of internal mass transfer limitations in governing co-substrate availability and overall reaction efficiency.

Figure 2a displays the influence of the dimensionless parameter φ^2 on $s(x)$ for a fixed $\alpha = 0.09$, $m_1 = 2$ and $\rho_1 = 0.5$. An increase in φ^2 results in higher substrate concentrations throughout the domain, signifying that increased reaction parameter values enhance substrate generation or reduce its depletion. Figure 2b illustrates the impact of the dimensionless parameter α on the normalized substrate concentration $S(x)$ along the catalyst bed for fixed values of $\varphi^2 = 1,\ m_1 = 2$ and $\rho_1 = 0.5$. As α increases from 0.01 to 0.05, the substrate concentration profile rises, indicating enhanced mass transport and accumulation of substrate along the bed length due to higher convection effects.

Figure 3a demonstrates the sensitivity of $L(x)$ to the variation in the reaction parameter φ^2 under fixed conditions of $\lambda = 0.5,\ m_2 = 0.5,\ \mu_2 = 1$. With increasing φ^2, a steeper decline in product concentration is observed, which reflects an intensifying reaction rate that consumes the product more rapidly within the catalytic bed. Figure 3b shows the variation of normalized medial product concentration $L(x)$ with respect to different values of the generation rate parameter λ, while keeping $\varphi^2 = 1,\ m_2 = 2$ and $\mu_2 = 1$ constant. As λ increases from 1 to 5, the product concentration decreases more steeply along x, suggesting a stronger decay or consumption mechanism influenced by the production term.

Figure 4a shows the variation of the normalised reducing agent concentration $R(x)$ with respect to the normalised current coordinate x for different values of $\varphi^2 = 0.5,\ 1,\ 3,\ 5,\ 7$, while keeping $\gamma = 1,\ m_3 = 0.1$ and $\mu_3 = 0.6$ constant. As φ^2 increases, the concentration of the reducing agent $R(x)$ decreases more steeply along the domain. Larger values of φ^2, the Thiele modulus increases the reaction rate relative to diffusion, resulting in more rapid depletion of the reducing agent. Figure 4b shows the effect of γ on $R(x)$ with fixed $\varphi^2 = 1,\ m_3 = 0.1,\ \mu_3 = 0.6$. As γ increases, the overall concentration level rises slightly, while the profiles remain nearly flat. This indicates that γ mainly alters the magnitude of $R(x)$ with minimal impact on its spatial variation.

Figure 5a explores the effect of the Thiele modulus squared φ^2 (ranging from 0.1 to 10) on the concentration profile. A higher φ^2 leads to a stronger decline in $C(x)$, suggesting increased diffusion limitations or higher reaction rates. The values of $\beta = 0.54,\ \rho = 0.1$ and $\mu_1 = 0.8$ are fixed during this variation. Figure 5b shows the influence of the parameter β on the co-substrate concentration profile. As β increases from 0.1 to 1, a linear enhancement in $C(x)$ is observed across the domain, indicating that higher β values support greater substrate availability. The parameters $\varphi^2 = 0.1,\ \rho = 0.1$ and $\mu_1 = 0.8$ are held constant. These figures illustrate how increasing β enhances substrate concentration, while increasing φ^2 suppresses it, highlighting the interplay between transport and reaction parameters.

Figure 6a shows the effect of α on normalised current Ψ versus β, with fixed $\varphi^2 = 5,\ \mu_1 = 1,\ \rho = 0.5$. Higher α values result in increased current and steeper profiles, indicating enhanced electrochemical activity. This reflects the role of α in boosting current response through improved transport or reaction kinetics. In Figure 6b Ψ varies linearly with ρ for different φ^2, with fixed $\alpha = 0.09,\ \mu_1 = 0.1,\ \beta = 0.5$. Larger φ^2 values produce higher currents, indicating stronger reaction dominance. The linear trend suggests a direct dependence of current on ρ modulated by reaction kinetics.

The parametric analysis and concentration profiles obtained from this model provide valuable, practical insights for optimizing the physical and chemical design of enzymatic catechol sensors. The Thiele modulus φ^2, identified as a key governing parameter, serves as an essential design criterion. A high φ^2 indicates reaction-dominated behaviour, resulting in steep concentration gradients and significant substrate depletion within the enzyme membrane. In practical terms, this means that for sensors aiming at low detection limits, a thinner enzyme layer or reduced enzyme loading should be used to lower φ^2, allowing complete substrate penetration and preventing the reaction from being confined to the surface region.

Conversely, when a higher current output is desired for a given analyte concentration, the model reveals that increasing parameters such as α and ρ enhances the normalized current Ψ. This can be practically achieved by improving the enzyme immobilization matrix to raise the apparent maximum reaction rate V_m or by increasing enzyme loading, thereby adjusting the interplay between kinetic and diffusion control.

Moreover, the nearly uniform profile of the reducing agent $R(x)$ at low φ^2 values indicates that the bulk concentration of L-ascorbate is sufficient to maintain the cyclic reaction without becoming a limiting factor, simplifying the preparation of the measurement medium. Overall, this mathematical model enables sensor designers to strategically choose membrane

thickness and enzyme loading in advance to achieve the desired balance of sensitivity, response time, and performance for specific clinical or environmental applications.

5. Conclusion

In this study, a mathematical model was developed to describe the behaviour of a tyrosinase-based amperometric biosensor operating via a cyclic redox mechanism between catechol and 1,2-benzoquinone, mediated by L-ascorbic acid. The coupled nonlinear reaction-diffusion equations, governed by a ping-pong enzymatic mechanism, were transformed into their dimensionless forms and solved analytically using the HPM. The derived analytical solutions for substrate, co-substrate, reducing agent, and intermediate product concentrations demonstrated excellent agreement with numerical simulations, with minimal relative errors across all species.

The impact of key dimensionless parameters-including the Thiele modulus, a critical indicator of the balance between reaction and diffusion-was systematically investigated. The Thiele modulus φ^2 emerged as a pivotal factor influencing reactant distribution and sensor response, with higher values indicating diffusion-limited behaviour. The current response, central to biosensor performance, showed a strong dependence on the interplay between mass transport and kinetic parameters.

The practical significance of this paper lies in its direct application to biosensor design and optimisation. The model provides precise, quantitative guidance for tuning key engineering parameters, such as enzyme membrane thickness and enzyme loading, by linking them directly to the Thiele modulus and current response. This allows for the rational design of sensors tailored for specific performance criteria, for instance, using a thinner membrane to enhance sensitivity for low-concentration detection, or increasing enzyme loading to amplify signal output. By moving beyond trial-and-error, this analytical framework enables the efficient development of more effective and reliable biosensors for practical applications in clinical diagnostics and environmental monitoring.

This article provides a valuable analytical framework for optimizing biosensor configurations involving cyclic enzymatic reactions. The approach facilitates a deeper understanding of system dynamics, enabling informed design strategies for enhanced sensitivity and rapid response in biomedical and environmental sensing applications. To build upon this theoretical foundation, the logical next steps include experimental validation of the model's predictions against real-world amperometric data. Furthermore, the model can be extended to incorporate more complex scenarios, such as multi-enzyme systems for cascaded signal amplification, the effects of enzyme inhibition, and the dynamics of oxygen limitation in thick-film sensors.

Conflict of interest

The authors declare no competing financial interest.

References

[1] Ramesh M, Janani R, Deepa C, Rajeshkumar L. Nanotechnology-enabled biosensors: A review of fundamentals, design principles, materials, and applications. *Biosensors*. 2022; 13(1): 40. Available from: https://doi.org/10.3390/bios13010040.

[2] Xue Y, Xie H, Wang Y, Feng S, Sun J, Huang J, et al. Novel and sensitive electrochemical/fluorescent dual-mode biosensing platform based on the cascaded cyclic amplification of enzyme-free DDSA and functional nucleic acids. *Biosensors and Bioelectronics*. 2022; 218: 114762. Available from: https://doi.org/10.1016/j.bios.2022.114762.

[3] Zhang G, Maeno Y, Iitani K, Arakawa T, Iwasaki Y, Toma K, et al. Enhanced sensitivity of a fluorometric biosensor for alcohol metabolites with an enzymatic cycling reaction. *Sensors and Actuators B: Chemical*. 2024; 401: 135031. Available from: https://doi.org/10.1016/j.snb.2023.135031.

[4] Mohanty SP, Kougianos E. Biosensors: A tutorial review. *IEEE Potentials*. 2006; 25(2): 35-40. Available from: https://doi.org/10.1109/MP.2006.1649009.

[5] Chaubey A, Gerard M, Singh VS, Malhotra BD. Immobilization of lactate dehydrogenase on tetraethylorthosilicate-derived sol-gel films for application to lactate biosensor. *Applied Biochemistry and Biotechnology*. 2001; 96: 303-311. Available from: https://doi.org/10.1385/ABAB:96:1-3:303.

[6] Das P, Das M, Chinnadayyala SR, Singha IM, Goswami P. Recent advances on developing 3rd generation enzyme electrode for biosensor applications. *Biosensors and Bioelectronics*. 2016; 79: 386-397. Available from: https://doi.org/10.1016/j.bios.2015.12.055.

[7] Tripathi MK, Nickhil C, Kate A, Srivastva RM, Mohapatra D, Jadam RS, et al. Biosensor: Fundamentals, Biomolecular Component, and Applications. In: *Advances in Biomedical Polymers and Composites*. Amsterdam, The Netherlands: Elsevier; 2023. p.617-633.

[8] Liao S, Tan Y. A general approach to obtain series solutions of nonlinear differential equations. *Studies in Applied Mathematics*. 2007; 119(4): 297-354. Available from: https://doi.org/10.1111/j.1467-9590.2007.00387.x.

[9] Saadatmandi A, Dehghan M, Eftekhari A. Application of He's homotopy perturbation method for non-linear system of second-order boundary value problems. *Nonlinear Analysis: Real World Applications*. 2009; 10(3): 1912-1922. Available from: https://doi.org/10.1016/j.nonrwa.2008.02.032.

[10] Kohli N, Lee I, Richardson RJ, Worden RM. Theoretical and experimental study of bi-enzyme electrodes with substrate recycling. *Journal of Electroanalytical Chemistry*. 2010; 641: 104-110. Available from: https://doi.org/10.1016/j.jelechem.2009.12.010.

[11] Uchiyama S, Hasebe Y, Shimizu H, Ishihara H. Enzyme-based catechol sensor based on the cyclic reaction between catechol and 1,2-benzoquinone, using L-ascorbate and tyrosinase. *Analytica Chimica Acta*. 1993; 276(2): 341-345. Available from: https://doi.org/10.1016/0003-2670(93)80402-7.

[12] He JH. Taylor series solution for a third order boundary value problem arising in architectural engineering. *Ain Shams Engineering Journal*. 2020; 11(4): 1411-1414. Available from: https://doi.org/10.1016/j.asej.2020.01.016.

[13] Abukhaled M. Variational iteration method for nonlinear singular two-point boundary value problems arising in human physiology. *Journal of Mathematics*. 2013; 2013: 720134. Available from: https://doi.org/10.1155/2013/720134.

[14] Abukhaled M. Green's function iterative approach for solving strongly nonlinear oscillators. *Journal of Computational and Nonlinear Dynamics*. 2017; 12(5): 051021. Available from: https://doi.org/10.1115/1.4036813.

[15] Tchier F, Inc M, Korpinar ZS, Baleanu D. Solutions of the time fractional reaction-diffusion equations with residual power series method. *Advances in Mechanical Engineering*. 2016; 8(10): 1687814016670867. Available from: https://doi.org/10.1177/1687814016670867.

[16] Nirmala K, Manimegalai B, Rajendran L. Steady-state substrate and product concentrations for non-michaelis-menten kinetics in an amperometric biosensor-hyperbolic function and padé approximants method. *International Journal of Electrochemical Science*. 2020; 15(6): 5682-5697. Available from: https://doi.org/10.20964/2020.06.09.

[17] Nebiyal A, Swaminathan R, Karpagavalli SG. Theoretical analysis of nanofluid's random diffusion with chemical reaction over a stretchable rotating disk using Homotopy Analysis Method. *AIP Conference Proceedings*. 2024; 3160(1): 160002. Available from: https://doi.org/10.1063/5.0225247.

[18] Wazwaz AM. A reliable modification of Adomian decomposition method. *Applied Mathematics and Computation*. 1999; 102(1): 77-86. Available from: https://doi.org/10.1016/S0096-3003(98)10024-3.

[19] Akbari MR, Ganji DD, Majidian A, Ahmadi AR. Solving nonlinear differential equations of Vanderpol, Rayleigh and Duffing by AGM. *Frontiers of Mechanical Engineering*. 2014; 9(2): 177-190. Available from: https://doi.org/10.1007/s11465-014-0288-8.

[20] Raja R, Swaminathan R. Mathematical analysis of nonlinear differential equations in polymer coated microelectrodes. *Contemporary Mathematics*. 2024; 5(2): 2569-2582. Available from: https://doi.org/10.37256/cm.5220244426.

[21] Swaminathan R, Saravanakumar R, Venugopal K, Rajendran L. Analytical solution of nonlinear problems in homogeneous reactions occur in the mass-transfer boundary layer: Homotopy perturbation method. *International Journal of Electrochemical Science*. 2021; 16(6): 210644. Available from: https://doi.org/10.20964/2021.06.51.

[22] Reena A, Raja R, Swaminathan R. Theoretical analysis of pre-steady state behaviour of non-linear double intermediate enzymatic reaction. *Contemporary Mathematics*. 2024; 5(2): 2089-2108. Available from: https://doi.org/10.37256/cm.5220244393.

Appendix A

The homotopy corresponding to the governing equation was systematically constructed for the equations (9)-(12) as follows

$$(1-p)\left(\frac{d^2s}{dx^2}\right)+p\left(\frac{d^2s}{dx^2}-\varphi^2\rho_1\left[\left(1+\frac{1}{s}+\frac{1}{C}\right)^{-1}-m_1LR\right]\right)=0 \tag{21}$$

$$(1-p)\left(\frac{d^2L}{dx^2}\right)+p\left(\frac{d^2L}{dx^2}-\varphi^2\mu_2\left[m_2L-\left(1+\frac{1}{S}+\frac{1}{C}\right)^{-1}\right]\right)=0 \tag{22}$$

$$(1-p)\left(\frac{d^2R}{dx^2}\right)+p\left(\frac{d^2R}{dx^2}-\mu_3m_3\varphi^2R\right)=0 \tag{23}$$

$$(1-p)\left(\frac{d^2C}{dx^2}\right)+p\left(\frac{d^2C}{dx^2}-\varphi^2\mu_1\rho\left[\left(1+\frac{1}{S}+\frac{1}{C}\right)^{-1}\right]\right)=0. \tag{24}$$

The following are the analytical solutions for the following equations (21)-(24)

$$S=S_0+pS_1+p^2S_2+\ldots \tag{25}$$

$$L=L_0+pL_1+p^2L_2+\ldots \tag{26}$$

$$R=R_0+RL_1+R^2L+\ldots \tag{27}$$

$$C=C_0+pC_1+p^2C_2+\ldots \tag{28}$$

Using the same powers of p-terms to arrange the results of substituting (25)-(28) into equations (21)-(24)

$$p^0:\frac{d^2S_0}{dx^2}=0,\ \frac{dS_0(1)}{dx^2}=0,\ \ S_0(0)=\alpha \tag{29}$$

$$p^0:\frac{d^2L}{dx^2}=0,\ \frac{dL(1)}{dx^2}=0,\ \ L_0(0)=\lambda \tag{30}$$

$$p^0:\frac{d^2R_0}{dx^2}=0,\ \frac{dR(1)}{dx^2}=0,\ \ R_0(0)=\gamma \tag{31}$$

$$p^0:\frac{d^2S_0}{dx^2}=0,\ C_0(1)==0,\ \ C_0(0)=\beta \tag{32}$$

$$p^1 : \frac{d^2 s_0}{dx^2} - \varphi^2 \rho_1 \left[\left(1 + \frac{1}{s} + \frac{1}{C} \right)^{-1} - m_1 LR \right] = 0,\ \frac{dS_1}{dx}(1) = 0,\ S_1(0) = 0 \tag{33}$$

$$p^1 : \frac{d^2 L_0}{dx^2} - \varphi^2 \mu_2 \left[m_2 L - \left(1 + \frac{1}{s} + \frac{1}{C} \right)^{-1} \right] = 0,\ \frac{dL_1}{dx}(1) = 0 \tag{34}$$

$$p^1 : \frac{d^2 R_0}{dx^2} - \mu_3 m_3 \varphi^2 R = 00,\ \frac{dR_1}{dx}(1) = 0,\ R_1(0) = 0 \tag{35}$$

$$p^1 : \frac{d^2 C_0}{dx^2} - \varphi^2 \rho_1 \left[\left(1 + \frac{1}{s} + \frac{1}{C} \right)^{-1} - m_1 LR \right] = 0,\ C_1(1) = 0,\ (C_1(0)). \tag{36}$$

The following outcome can be attained by solving (32)-(33)

$$S_0 = \alpha,\ L_0 = \lambda\ R_0 = \gamma,\ C_0 = \beta$$

$$S_1 = \varphi^2 \rho_1 \left(\frac{-\alpha\beta}{\alpha\beta + \alpha + \beta} + m_1 \lambda \gamma \right) \left(x - \frac{x^2}{2} \right)$$

$$L_1 = \varphi^2 m_2 \left(\frac{\alpha\beta m_2 + \alpha\lambda m_2 + \beta\lambda m_2 - \alpha\beta}{\alpha\beta + \alpha + \beta} \right) \left(\frac{x^2}{2} - x \right)$$

$$R_1 = \varphi^2 m_3 \mu_3 \gamma \left(x^2 - x \right)$$

$$C_1 = \left(\frac{\varphi^2 \mu_1 \rho \alpha\beta}{(\beta + 1)\alpha + \beta} \right) \left(\frac{x^2}{2} - x \right)$$

$$S(x) = \alpha + \varphi^2 \rho_1 \left(\frac{-\alpha\beta}{\alpha\beta + \alpha + \beta} + m_1 \lambda \gamma \right) \left(x - \frac{x^2}{2} \right) \tag{37}$$

$$L(x) = \lambda + \varphi^2 m_2 \left(\frac{\alpha\beta m_2 + \alpha\lambda m_2 + \beta\lambda m_2 - \alpha\beta}{\alpha\beta + \alpha + \beta} \right) \left(\frac{x^2}{2} - x \right) \tag{38}$$

$$R(x) = \gamma + \varphi^2 m_3 \mu_3 \gamma \left(x^2 - x \right) \tag{39}$$

$$C(x) = -\beta x + \beta + \left(\frac{\varphi^2 \mu_1 \rho \alpha\beta}{(\beta + 1)\alpha + \beta} \right) \left(\frac{x^2}{2} - x \right). \tag{40}$$

The solution can be represented by HPM as follows

$$S(x) = \lim_{p\to 1} S_0 + S_1 = \alpha + \varphi^2 \rho_1 \left(\frac{-\alpha\beta}{\alpha\beta + \alpha + \beta} + m_1 \lambda \gamma \right) \left(x - \frac{x^2}{2} \right) \tag{41}$$

$$L(x) = \lim_{p\to 1} L_0 + L_1 = \lambda + \varphi^2 m_2 \left(\frac{\alpha\beta m_2 + \alpha\lambda m_2 + \beta\lambda m_2 - \alpha\beta}{\alpha\beta + \alpha + \beta} \right) \left(\frac{x^2}{2} - x \right) \tag{42}$$

$$R(x) = \lim_{p\to 1} R_0 + R_0 = \gamma + \varphi^2 m_3 \mu_3 \gamma \left(x^2 - x \right) \tag{43}$$

$$C(x) = \lim_{p\to 1} C_0 + C_0 = -\beta x + \beta + \left(\frac{\varphi^2 \mu_1 \rho \alpha\beta}{(\beta+1)\alpha + \beta} \right) \left(\frac{x^2}{2} - x \right). \tag{44}$$